AFRL-RH-BR-TR-2007-0074

Conduction and Convection of Heat Produced by the Attenuation of Laser Beams in Liquids

Irwin S. Goldberg
Misty Garcia

St. Mary's University

Sahar Maswadi

University of Texas Health Science Center

Robert J. Thomas

Air Force Research Laboratory

Clifton D. Clark III

Northrop Grumman
Information Technology

September 2007

Air Force Research Laboratory
Human Effectiveness Directorate
Directed Energy Bioeffects Division
Optical Radiation Branch
Brooks-City-Base, TX 78235

NOTICE AND SIGNATURE PAGE

Using Government drawings, specifications, or other data included in this document for any purpose other than Government procurement does not in any way obligate the U.S. Government. The fact that the Government formulated or supplied the drawings, specifications, or other data does not license the holder or any other person or corporation; or convey any rights or permission to manufacture, use, or sell any patented invention that may relate to them.

This report was cleared for public release by the Air Force Research Laboratory, Brooks City-Base, Public Affairs Office and is available to the general public, including foreign nationals. Copies may be obtained from the Defense Technical Information Center (DTIC) (http://www.dtic.mil).

AFRL-RH-BR-TR-0074 HAS BEEN REVIEWED AND IS APPROVED FOR PUBLICATION IN ACCORDANCE WITH ASSIGNED DISTRIBUTION STATEMENT.

//SIGNED//
ROBERT J. THOMAS, DR-IV
Contract Monitor

//SIGNED//
GARRETT D. POLHAMUS, DR-IV, DAF
Chief, Directed Energy Bioeffects Division

This report is published in the interest of scientific and technical information exchange, and its publication does not constitute the Government's approval or disapproval of its ideas or findings.

REPORT DOCUMENTATION PAGE

Form Approved
OMB No. 0704-0188

1. REPORT DATE (DD-MM-YYYY)	2. REPORT TYPE	3. DATES COVERED (From - To)
September 2007	Final Technical Report	July 2006- September 2007

4. TITLE AND SUBTITLE

Conduction and Convection of Heat Produced by the Attenuation of Laser Beams in Liquids

5a. CONTRACT NUMBER
FA8650-06-1-6747

5b. GRANT NUMBER
10-2118-4450-G503

5c. PROGRAM ELEMENT NUMBER
62202F

6. AUTHOR(S)
[+]Goldberg, Irwin S.; [+]Garcia, Misty; [#]Maswadi, Saher; [◊]Thomas, Robert J.; [□]Clark, Clifton.D.

5d. PROJECT NUMBER
7757

5e. TASK NUMBER
B2

7. PERFORMING ORGANIZATION NAME(S) AND ADDRESS(ES)

[+]St. Mary's University
Engineering Department
San Antonio, TX 78228

[◊]Air Force Research Laboratory
Human Effectiveness Directorate
Directed Energy Bioeffects Division
2624 Louis Bauer Dr.
Brooks City-Base, TX 78235-5128

[□]Northrop Grumman Corporation
Information Technology
4241 Woodcock Drive, Ste B-100
San Antonio, TX 78228

[#]University of Texas Health Science Center
Ophthalmology Department
San Antonio, TX

5f. WORK UNIT NUMBER
33

8. PERFORMING ORGANIZATION REPORT NUMBER

9. SPONSORING / MONITORING AGENCY NAME(S) AND ADDRESS(ES)

Air Force Materiel Command
Human Effectiveness Directorate
Directed Energy Bioeffects Division
Optical Radiation Branch
2624 Louis Bauer Dr.
Brooks City-Base, TX 78235-5128

10. SPONSOR/MONITOR'S ACRONYM(S)
AFRL/RH

11. SPONSOR/MONITOR'S REPORT NUMBER(S)
AFRL-RH-BR-TR-2007-0074

12. DISTRIBUTION / AVAILABILITY STATEMENT

Approved for public release; distribution unlimited.

13. SUPPLEMENTARY NOTES

Contract Monitor: Dr. Robert. J. Thomas

14. ABSTRACT

Mathematical models are used to simulate temperature changes that are induced by the absorption of energy from propagating laser beams in water. Both convective and conductive heat transfer are considered. Thermally insulated surfaces as well as surfaces involving heat transfer with the surroundings are considered. The simulated results demonstrate the importance of thermal convection.

In the first part of this report, containers with closed surfaces are considered. In the second part of the report, free-surface effects are considered: These effects include evaporative heat loss and the occurrence of surface tension produced by temperature gradients at the surface (the Marangoni effect). Evaporative heat loss is simulated and the Marangoni effect is discussed.

The quantitative determination of the temperature changes in the water, due to the heat transferred by an absorbed laser beam, could facilitate the improvement of models involving the optics of laser beam penetration in liquids.

15. SUBJECT TERMS

Laser Absorption, Navier-Stokes Equation, Heat Conduction, Thermal Convection, Convective Currents, Marangoni Effect, Heat Transport, Evaporative Losses, Energy Conservation, Surface Tension, Laser Optics, Thermal Modeling

16. SECURITY CLASSIFICATION OF:			17. LIMITATION OF ABSTRACT	18. NUMBER OF PAGES	19a. NAME OF RESPONSIBLE PERSON
a. REPORT	b. ABSTRACT	c. THIS PAGE			Dr. Robert J. Thomas
Unclassified	Unclassified	Unclassified	SAR	43	19b. TELEPHONE NUMBER (include area code)

Standard Form 298 (Rev. 8-98)

This page intentionally left blank.

TABLE OF CONTENTS

FIGURES

TABLES

1. INTRODUCTION

Mathematical modeling and experimental methods have been used by researchers to understand the optical effects of laser beam penetration in the aqueous humor. These models and experiments reveal the phenomena of thermal lensing of the laser beam [Vincelette, et. al, 2007].

Water is heated by the power absorbed from an attenuated laser beam. The temperature changes of the heated water cause localized refractive-index changes in the propagating medium. Therefore, a quantitative analysis of local temperature changes caused by the laser heating could facilitate a better understanding of the laser lensing effects.

Laser heating is caused by coupled convective and conductive transport of thermal energy. The experimental results of Vincelette, *et. al.* [2007] suggests the importance of thermal convection upon the optical properties of laser beam penetration.

When conductive effects predominate, and convective effects are negligible, the thermal changes can be observed as circularly-symmetric temperature profiles. Circularly asymmetric temperature patterns can be observed when the convective effects become relevant.

In this report, simulation results for laser heating of water will be presented, and the conductive and convective heating effects will be evaluated.

This page intentionally left blank

2. SIMULATION OF CONDUCTIVE AND CONVECTIVE HEAT TRANSFER AND TEMPERATURE CHANGES DUE TO LASER HEATING OF WATER: MATHEMATICAL AND THEORETICAL BACKGROUND

2.1 BASIC PRINCIPLES AND MATHEMATICAL EQUATIONS

Thermal heating is modeled using the thermal transport equation coupled with the Navier-Stokes and continuity equations. The thermal transport equation describes temperature changes caused by thermal convection and conduction, while the Navier-Stokes and continuity equations describe the convective velocity caused by spatial variations of the buoyancy force. The spatial variations in the buoyancy force result from temperature-dependent density gradients. Thus, the Navier-Stokes, continuity, and thermal transport equations form a set of coupled, partial - differential equations from which the fluid convective transport and the temperature variations can be determined.

The fluid flow is governed by the Navier-Stokes equations [Landau and Lifshitz,1959; Batchelor, 1967]:

$$\rho\frac{\partial\vec{V}}{\partial t}+\rho(\vec{V}\bullet\nabla)\vec{V}+\nabla P-\eta\nabla^2\vec{V}=\vec{F}, \tag{1}$$

and the continuity condition for incompressible flow

$$\nabla\bullet\vec{V}=0, \tag{2}$$

where ρ denotes the density, and η denotes the dynamic viscosity of the liquid, t denotes time and $\vec{F}$ denotes the body force caused by spatially varying buoyancy effects.

The equation for conductive and convective heat transfer is

$$\rho C\left(\frac{\partial T}{\partial t}+\vec{V}\bullet\nabla T\right)-\nabla\bullet\left(k\ \nabla T\right)=\dot{Q}_S\ , \tag{3}$$

where C is the specific heat (J / kg•K) and k is the thermal conductivity of the liquid (W/(m•K)). $\dot{Q}_S$ is a heat-source term (W/m^3), and T is the temperature (K) [Incropera, et al, 2007].

The heat-source term, $\dot{Q}_S$, denotes the heat absorbed (per unit volume) by the laser. This term can be expressed as [Torres et al, 1993].

$$\dot{Q}_S(r,z,t)=\mu_a\left|\vec{S}(r,z,t)\right|, \tag{4}$$

where μ_a is the absorption coefficient of the material (m^{-1}). Using Beer's law as a first approximation, the magnitude of the laser energy flux is given as

$$\left|\vec{S}(r,z,t)\right| = \frac{P}{\pi {R_w}^2}\exp\left(\frac{-(r-r_0)^2}{{R_w}^2}\right)\exp(-\mu_a z)\, f(t)\ . \tag{5}$$

Here, *P* is the power of the incident laser beam* (W), R_W is the e^{-1} laser beam radius (m), r is the radial coordinate and z is the axial coordinate. The position of the central axis of the laser beam is denoted as r_0. When rectangular coordinates (x,y,z) are used, with a center axis at (x_0,y_0), $r - r_0$ is given as

$$r - r_0 = \sqrt{(x-x_0)^2 + (y-y_0)^2}\ . \tag{5a}$$

To model transient effects from a continuous-wave laser, $f(t)$ is a unit-step function.

The Boussinesq approximation, which is explained in the next paragraph, is used to determine the effect of temperature gradients upon the convective velocity of the liquid. The temperature-dependent density variations produce spatial variations of the buoyant force within the liquid. Thus, the x and y components of the gravitational body-force, F, are

$$\begin{aligned} F_x &= 0, \\ F_y &= -g\ \rho(T) \end{aligned} \tag{6}$$

where g is the acceleration of gravity (9.81 m/s^2), $\rho(T)$ is the temperature-dependent density of the liquid (kg/m^3). A plot of density, $\rho(T)$ verses temperature, T. for water is shown in Figure 1 [Comsol Lib., 2006].

* To determine the incident laser power P, the reflection losses at the front face must be taken into account. Thus, P is equal to the power of the laser multiplied by the fraction of the laser power that is transmitted through the front face of the container.

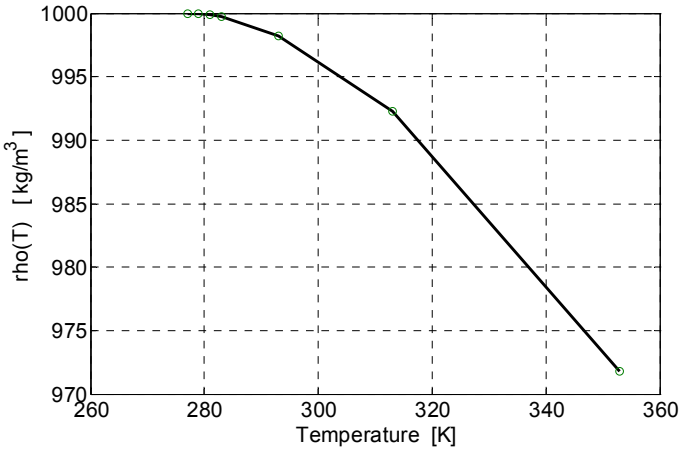

Figure 1. A plot of density versus temperature of water is shown.

Equation (6) is substituted into the body-force term at the right of the equal sign in equation (1). Note that, as indicated by equation (6), the body-force term in the Navier-Stokes equation (1) is temperature dependent. Also, the convective term in the heat-transport equation (3) is velocity dependent. Thus, equations (1), (2) and (3) form a coupled set of partial differential equations.

The Boussinesq approximation is used to determine the effect of temperature gradients upon the convective velocity of the liquid [Acheson, 1990; Drazin and Reid, 1981; Incropera, et al, 2007; Tritton, pp. 188-195, 1998]. According to the Boussinesq approximation, all density parameters in the equations (1) and (3) are constants (where ρ = 100 0kg/m^3), with the exception of the density variations involved with the buoyant force, which is included as a body-force term in the Navier-Stokes equation. The components of the temperature-dependent body-force are given by equation (6). The incompressibility condition, given by equation (2), is included as part of the Boussinesq approximation.

2.2 DIMENSIONLESS PARAMETERS:

Dimensionless parameters involved in convective and conductive heat and mass transport of an incompressible fluid are the Reynolds number and the Rayleigh number. The Reynolds number, Re, is expressed as

$$\mathrm{Re} = \frac{\overline{V}\rho\, d}{\eta}, \qquad (7)$$

Where $\overline{V}$ denotes the velocity scale, and d denotes the length scale (equal to a length of a side of the container). Also, ρ denotes the density, and η denotes the dynamic viscosity of the liquid. The Reynolds number expresses the order-of-magnitude estimate of the ratio of the inertia terms

to the viscous term in the Navier-Stokes equation. High Reynolds numbers indicate flow instability for transition to turbulence [Landau and Lifshitz,1959]. In our investigation, the calculated Reynolds numbers are on the order of 1 – 10, indicating the non-existence of turbulence, but also indicating that the non-linear term and the time-dependent term in the Navier-Stokes equation cannot be neglected.

The Rayleigh number, *Ra*, given as

$$Ra = \frac{g\alpha(\Delta T){d_T}^3\rho}{\eta\kappa}, \tag{8}$$

where g is the acceleration of gravity (9.81 m/s^2), α is the thermal expansion coefficient of the liquid (K^{-1}), ΔT is the magnitude of the spatial variation of temperature (K), and d_T denotes the length scale over which the thermal gradients are effective. The thermal diffusitivity of the fluid, κ (m^2/s), is given as

$$\kappa = \frac{k}{\rho C}. \tag{9}$$

The Rayleigh number indicates the instability of a heated liquid to the formation of convective flow. That is, at high Rayleigh numbers, convective flow is expected to occur. (For example, for flow between two rigid horizontal plates, separated by a vertical distance d_T, instabilities leading to convective flow occur when *Ra* exceeds a critical Rayleigh number of 1708 [Velarde, M.G., and Normand, 1980; Drazin and Reid,1981]. A critical value of the Rayleigh number corresponding to the physics and geometry of the problems considered in this report is not known.) As indicated by equations (8) and (9), an increase in the dynamic viscosity and/or in the thermal diffusitivity of the fluid would inhibit the formation of convective thermal flow.

Of course, for the problems considered in this report, neither the Reynolds number nor the Rayleigh number can be determined *a-priori*; the convective velocity term in the Reynolds number and the temperature difference term in the Rayleigh number must be determined as solutions to the problem.

2.3 SIMULATION PARAMETERS:

The simulation results for conductive and convective heat exchange are obtained using COMSOL Software, in which finite-element techniques are used with the Galerkin method [Reddy and Gartling, 2001; Zimmerman, 2006]. Computational results are given in the next few chapters: Results for a two-dimensional problem are given in chapter 3. Results for three-dimensional problems are given in chapter 4. Results for the three-dimensional problem I, in which all boundaries are thermally insulated, are given in section 4.1. Results for the three-dimensional problem II, in which heat transfer takes place at the front surface and all other surfaces are thermally insulated, are given in section 4.2. Free-surface affects are discussed in chapter 5. Evaporative effects are discussed in section 5.1, and Marangoni effects, involving thermally-induced surface tension, are discussed in section 5.2.

In the simulations described in chapters 3 and 4 of this report, the following assumptions and approximations are made:

1. Light scattering is negligible compared to absorption.
2. The Boussinesq approximation is used with the incompressibility condition for the fluid.
3. Non-slip boundary conditions (with zero velocity) apply to all surfaces.
4. Viscous dissipative losses are negligible.
5. Temperature variations of η, k, and C are not considered. (First Approximation) The parameters representing the dynamic viscosity, thermal conductivity and specific heat of the liquid are considered as constants with the values listed in table 1.

The parameters defining all simulations of chapters 3 and 4 are given in table 1.

Table 1. Parameter values used for all two-dimensional and three-dimensional heat conduction/convection problems [COMSOL Lib, 2007]

Parameter name	Symbol	Value	Units
dynamic viscosity	η	$9(10^{-4})$	kg/(m•s)
thermal conductivity	k	0.6114	W/(m•K)
specific heat	C	4200	J/(kg•K)
incident laser power	P	1	W
e^{-1} beam radius	R_W	$1.5(10^{-3})$	m
absorption coefficient	μ_a	150	m^{-1}
Density of water	ρ (**)	1000	Kg/m^3

** According to the Boussinesq approximation, ρ is constant, with the exception of the buoyant body-force term given by equation (6).

To approximate the Rayleigh number of water for small temperature variations, ΔT, around 295 K, the coefficient of thermal expansion, α, of $3(10^{-4})$ [K^{-1}], and g equal to 9.81 m/sec^2 are used. For the model described in this chapter, the order of the distance over which temperature variations are significant, is taken as $d_T = 10^{-2}$ meters. These values and the values of the parameters given in table 1 are substituted into equations (8) and (9) to obtain an approximation of the Rayleigh number in terms of the temperature variation, ΔT. The approximate result is

$$Ra \approx 2.7(10^4)\,\Delta T, \qquad (10)$$

where ΔT is given in units K. As indicated by equation (10), large values of the Rayleigh number exist for small temperature variations. This suggests the presence of convective flow for the temperature variations within the size of the container considered in this report.

This page intentionally left blank

3. SIMULATION OF HEAT TRANSPORT WHEN A HORIZONTAL LASER BEAM IS NORMAL TO A TWO-DIMENSIONAL PLANE SURFACE:

For illustrative purposes, a two-dimensional problem is first considered. This problem involves the simulation of heat transport when the heat source consists of a horizontal laser beam that is normal to and at the center of a two-dimensional plane surface. The heat source is represented by equations (4) and (5) where the term describing exponential decay in z (the $e^{-\mu_a z}$ term in equation (5) is set equal to one. For this problem, non-slip (zero-velocity) fluid-dynamic boundary conditions and thermally-insulated thermal boundary conditions exist on all surfaces. The initial temperature is 293.15 K, and the initial velocity everywhere is zero.

The simulated results are obtained using Comsol finite-element software with 24,656 degrees of freedom; 1,925 mesh points; and 3,728 triangular elements.

The geometry is shown in Figure 2. The temperature profiles at times equal to one and three seconds are shown in figures 3 and 4 respectively. The horizontal centerlines are drawn in these figures to demonstrate the vertical asymmetry of the temperature profile and to thereby illustrate the vertical convective effects of the heat transfer. The vertical centerlines are drawn to illustrate the horizontal symmetry of the temperature profile. A convective flow pattern is shown to exist at time equal to three seconds.

Convective velocity vectors are shown at time equals three seconds in figure 5. Note the closed paths formed by the flow vectors; this property is consistent with the solenoidal properties of the velocity vector, as indicated by equation (2).

Temperature profiles, as functions of y, along the central vertical axis (where x=0.01m) at various times are shown in figure 6. Note that the temperature profile is almost symmetric about the central vertical position (y = 0.01 m) at time equal to 0.3 seconds. However, as time increases, the vertical asymmetry of the temperature profile about the central horizontal position increases. This asymmetry illustrates the occurrence of convective heat transfer.

Temperature profiles, as functions of x, along the central horizontal axis (where y = 0.01m) at various times are shown in figure 7. These plots are used to check the results for the expected left-right symmetry properties of the solutions.

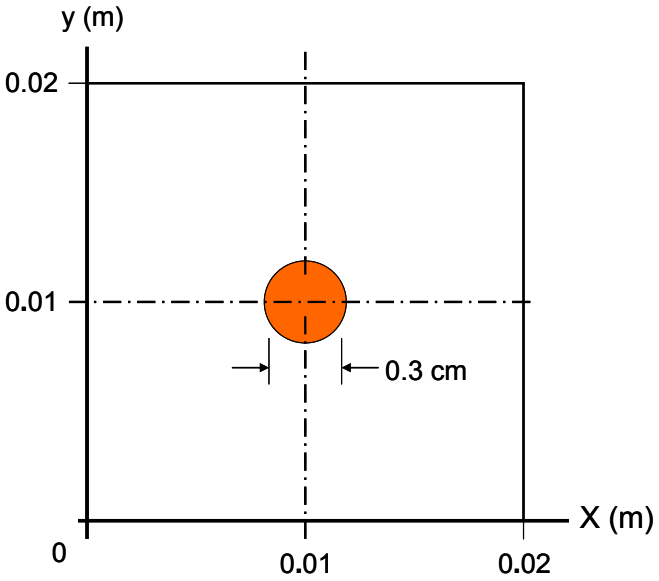

Figure 2. The geometry for the two-dimensional problem is shown. The laser beam (with its e^{-1} radius) is illustrated by the solid circle. All boundaries are thermally insulated, and the fluid velocity at all boundaries is zero (the non-slip boundary condition applies).

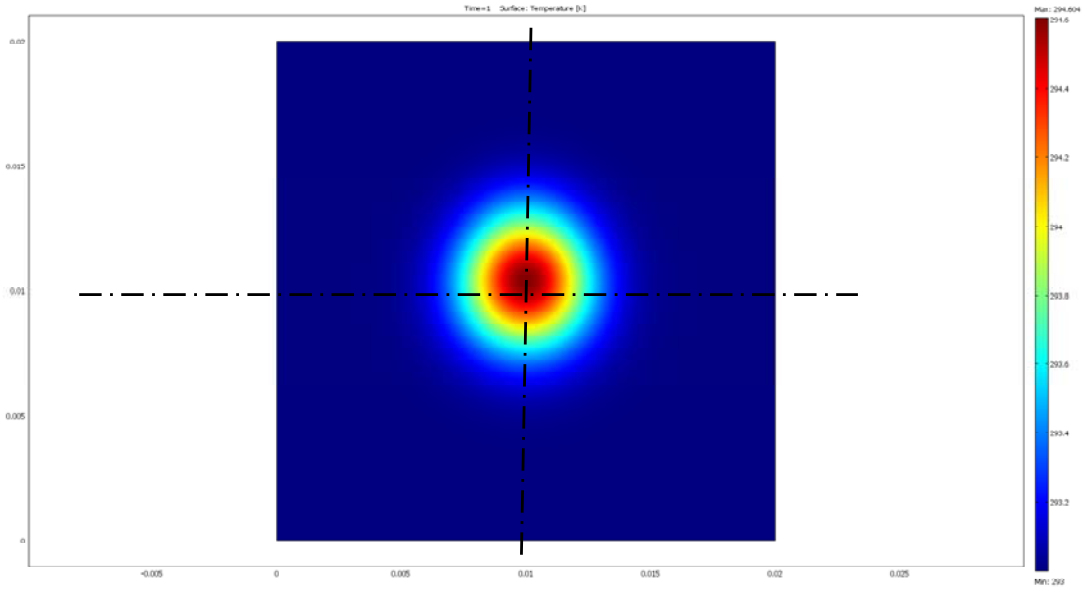

Figure 3. Results for the two-dimensional problem are shown. The temperature profile is given at time equals one second. Minimum temperature equals 293 K; maximum temperature equals 294.6 K. The horizontal centerline is drawn to indicate the slight vertical asymmetry of the temperature distribution; this illustrates an early stage of convective flow.

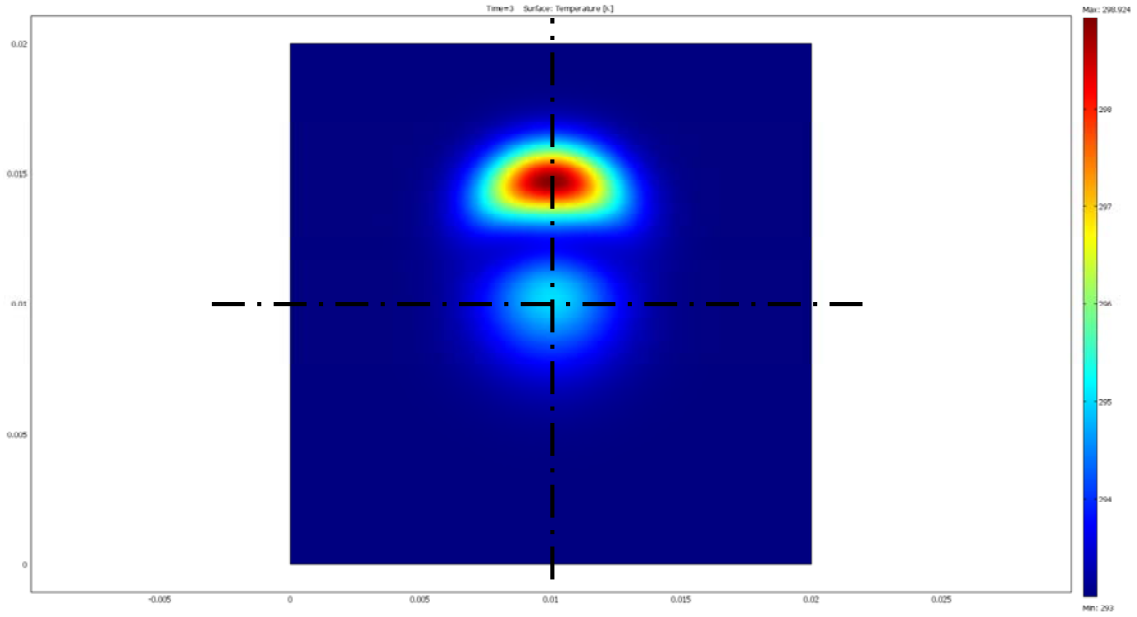

Figure 4. Results for the two-dimensional problem are shown. The temperature profile at time equals three seconds is given. Minimum temperature equals 293 K; maximum temperature equals 299 K. The horizontal centerline is drawn to indicate the vertical asymmetry of the temperature distribution; this illustrates effects of convective flow.

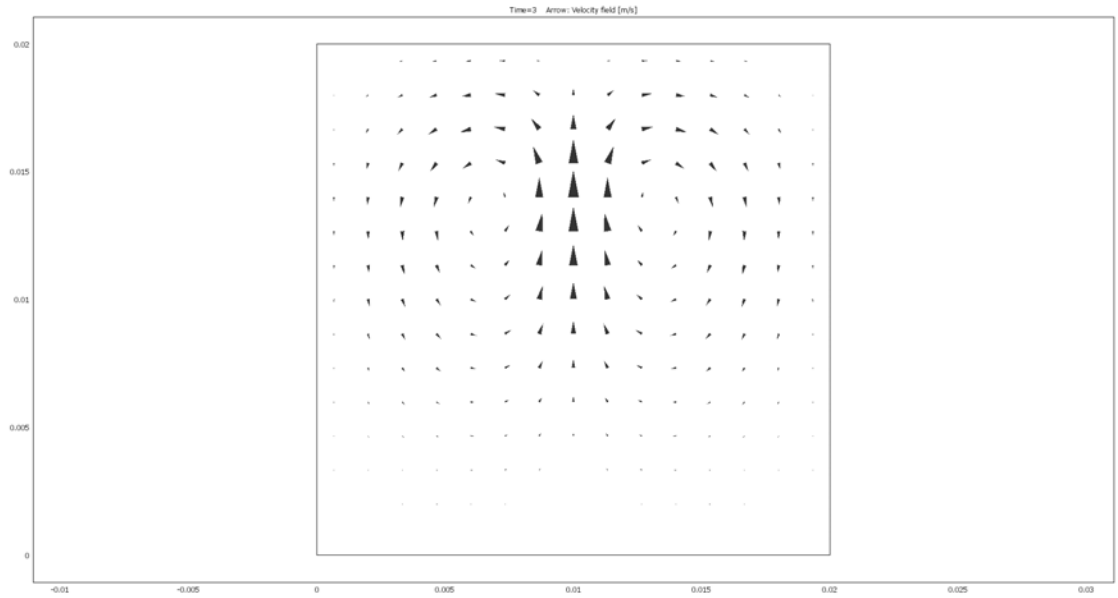

Figure 5. Results for the two-dimensional problem are given. Convective fluid velocity vectors at time t = 3s are shown. Note the convective flow profile. The maximum amplitude of the velocity is 4.4 mm/sec.

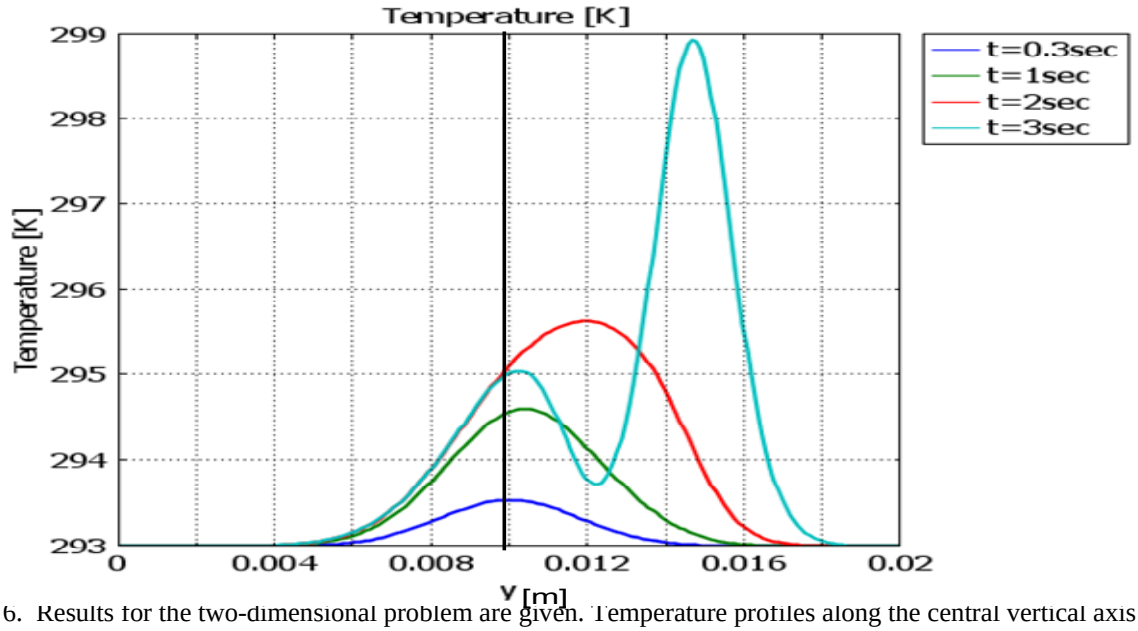

Figure 6. Results for the two-dimensional problem are given. Temperature profiles along the central vertical axis (where x = 0.01 m) are shown at various times. The asymmetry (about the center-y-position at y = 0.01 m) of the temperature in the y-direction is indicative of convective flow. This asymmetric pattern is shown to increase with time.

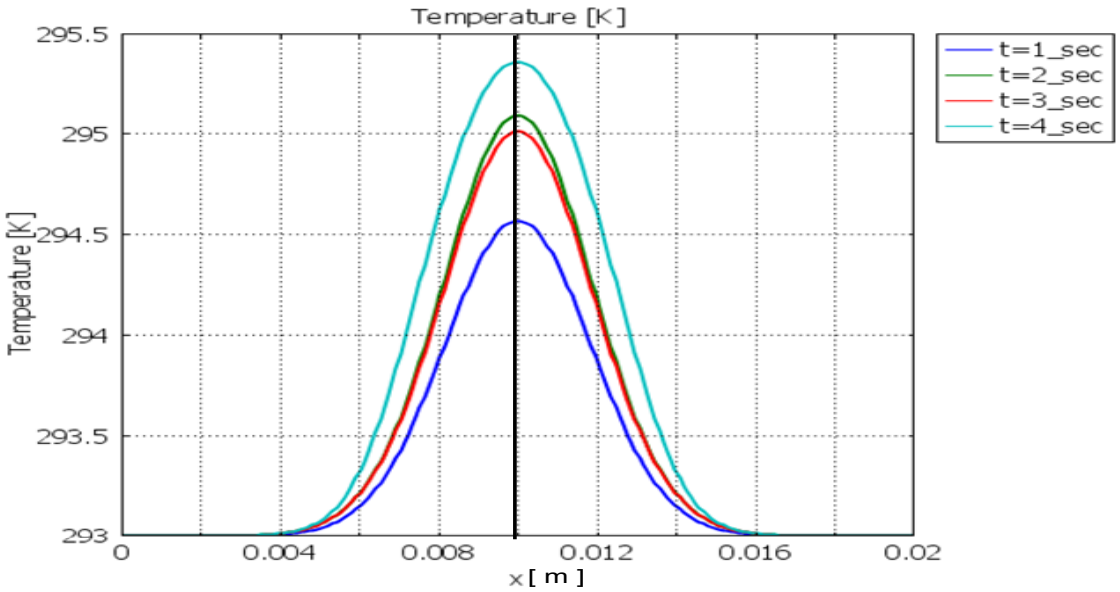

Figure 7. Results for the two-dimensional problem are given. Plots are shown of temperature profiles along the central horizontal axis (where y = 0.01 m) at various times. These results are presented to demonstrate the extent of the right-left symmetry (about the central-x position at x = 0.01 m) of the result.

4. SIMULATION OF HEAT TRANSPORT WHEN A HORIZONTAL LASER BEAM IS NORMAL TO A PLANE SURFACE OF A THREE-DIMENSIONAL RECTANGULAR CONTAINER

4.1 THREE-DIMENSIONAL PROBLEM 1: SIMULATION APPLIED TO THERMAL BOUNDARY CONDITIONS IN WHICH ALL SURFACES ARE THERMALLY INSULATED

For the three-dimensional problem 1 considered in this chapter, thermally-insulated thermal boundary conditions are specified on all surfaces. Also, non-slip fluid-dynamic boundary conditions are specified on all surfaces. The x-y faces are perpendicular to the laser beam. The laser beam enters perpendicularly to the front face at z = 0, and the laser penetrates with exponential decay in the z-direction (Beer's Law). As illustrated in figure 8, the faces perpendicular to the laser beam are specified with dimensions $0 \le x \le 0.02$ m, and $0 \le y \le 0.02$ m and the penetration distance extends from z = 0 to z = 0.04 m. The initial temperature is 293.15K, and everywhere the initial velocity is zero.

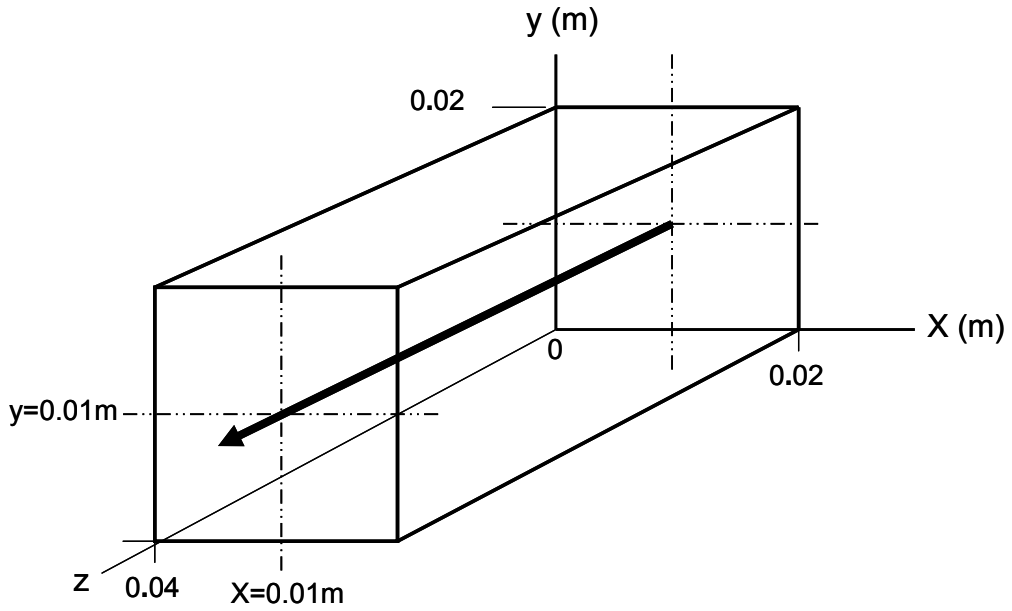

Figure 8. The geometry for the three-dimensional problems 1 and 2 is illustrated. The arrow shows the direction of propagation and attenuation of the laser beam. The coordinates are shown in meters, where $0 \le x \le 0.02$ m, $0 \le y \le 0.02$ m, and $0 \le z \le 0.04$m.

The simulated results are obtained using Comsol finite-element software with 27,793 degrees of freedom; 969 mesh points; and 4310 tetrahedral elements.

The temperature profile at the front face (where z = 0) at time equals four seconds is shown in figure 9. A horizontal centerline is drawn to illustrate the vertical asymmetry of the temperature profile. The temperature profile through a central y-z plane (where x = 0.01m) at time equals 4 seconds is shown in figure 10.

Temperature profiles, as functions of y, along the vertical central axis (where x = 0.01m) at the front face (z = 0) at various times are shown in figure 11. The temperature profile is almost vertically symmetric (about the central y position at y = 0.01m) at time equals one second. However, the vertical asymmetry of the temperature profile is shown to increase with increasing time.

Temperature profiles, as functions of y, along the central vertical axis (where x = 0.01m) at time equals three seconds are shown for various values of z in figure 12. Note the asymmetry in the y-direction. The vertical asymmetry of the temperature profiles, as shown in figures 9 to 12, are indicative of thermal convective effects.

Temperature profiles, as functions of x, along the central horizontal axis (where y = 0.01m) at time equals three seconds are shown for various values of z in figure 13. These results are plotted as a check to determine the horizontal symmetry of the solution. As expected, these results show that the solutions are close to being symmetric in the horizontal direction about the central horizontal position (at x = 0.01m). The small deviation from perfect symmetry in the x-direction is believed to be caused by a small computational inaccuracy.

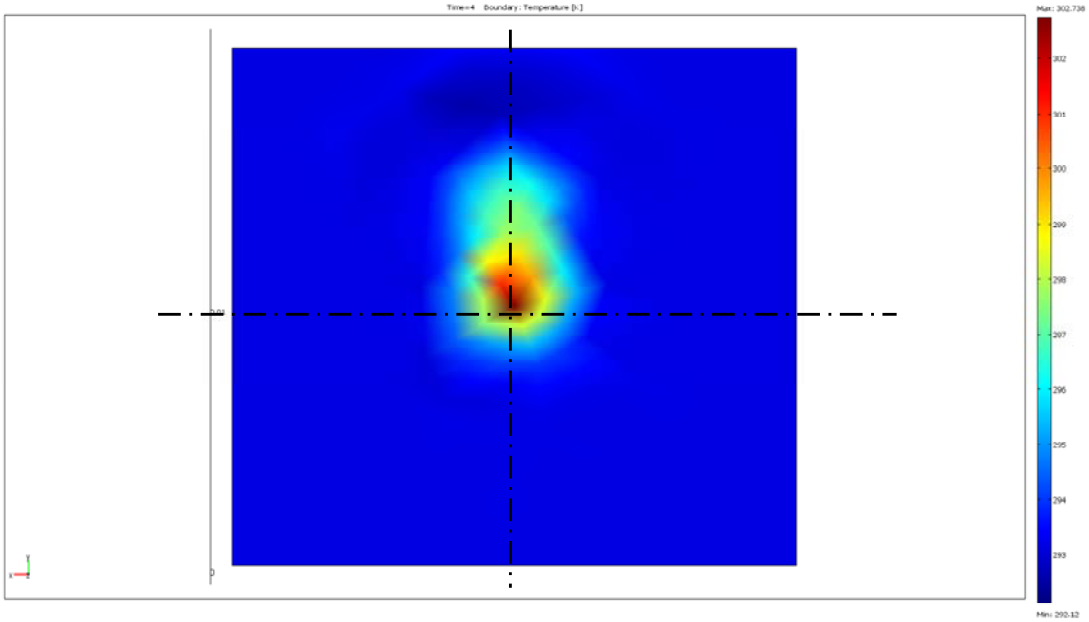

Figure 9. Results for the three-dimensional problem 1 are given. The temperature profile at the front face is shown at t = 4s. A horizontal centerline is drawn to illustrative vertical asymmetry caused by convection. A vertical centerline is drawn to evaluate the expected symmetry in the horizontal direction. Maximum temperature equals 302.7 K; minimum temperature equals 293.15 K

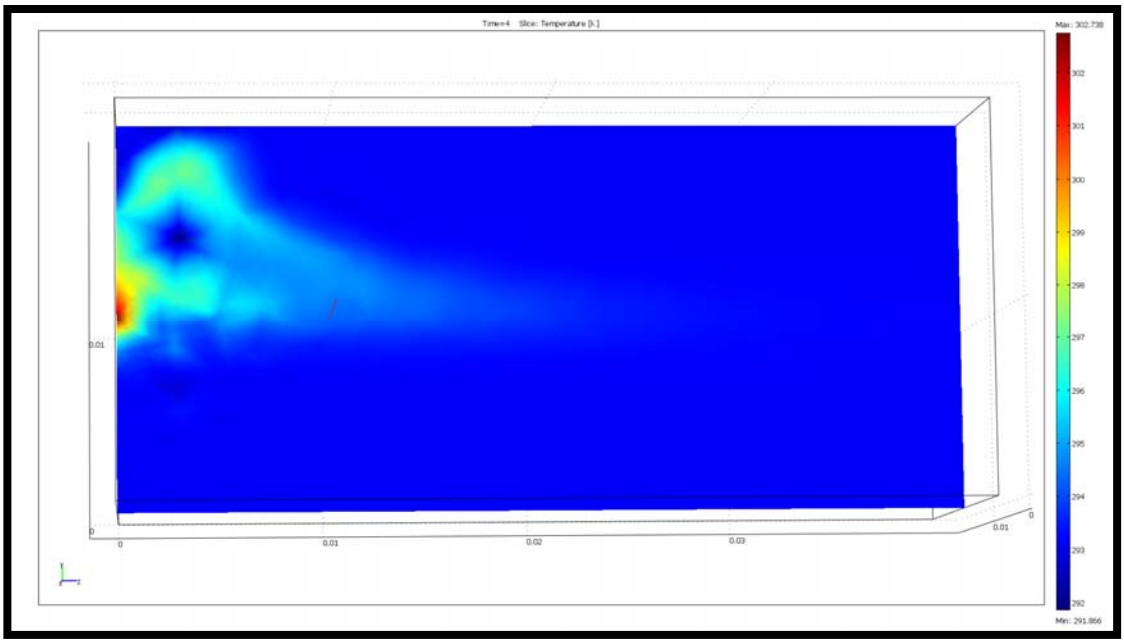

Figure 10. Results for the three-dimensional problem 1 are given. The temperature profile through a central y-z plane (where x = 0.01m) at t = 4s is presented. Note the vertical asymmetry of the temperature profile. Maximum temperature equals 302.8K; minimum temperature equals 293.15 K.

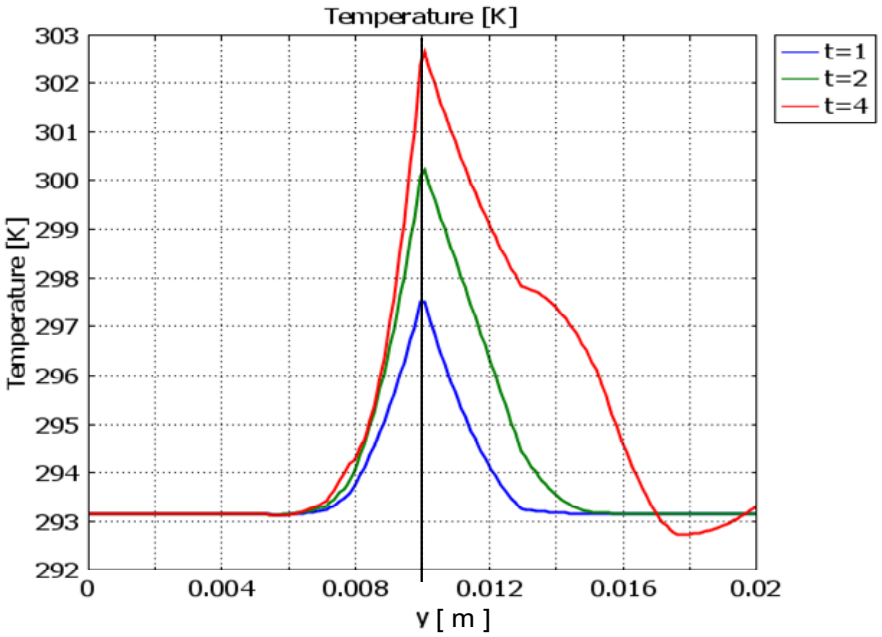

Figure 11. Results for the three-dimensional problem 1 are given. Temperature profiles along the vertical central axis (where x = 0.01m) at the face (z = 0) at various times are presented. Note the increase in the vertical asymmetry of the temperature about the central y position (at y = 0.01 m) with increasing time. The dip in temperature below 293K is caused by a small computational inaccuracy.

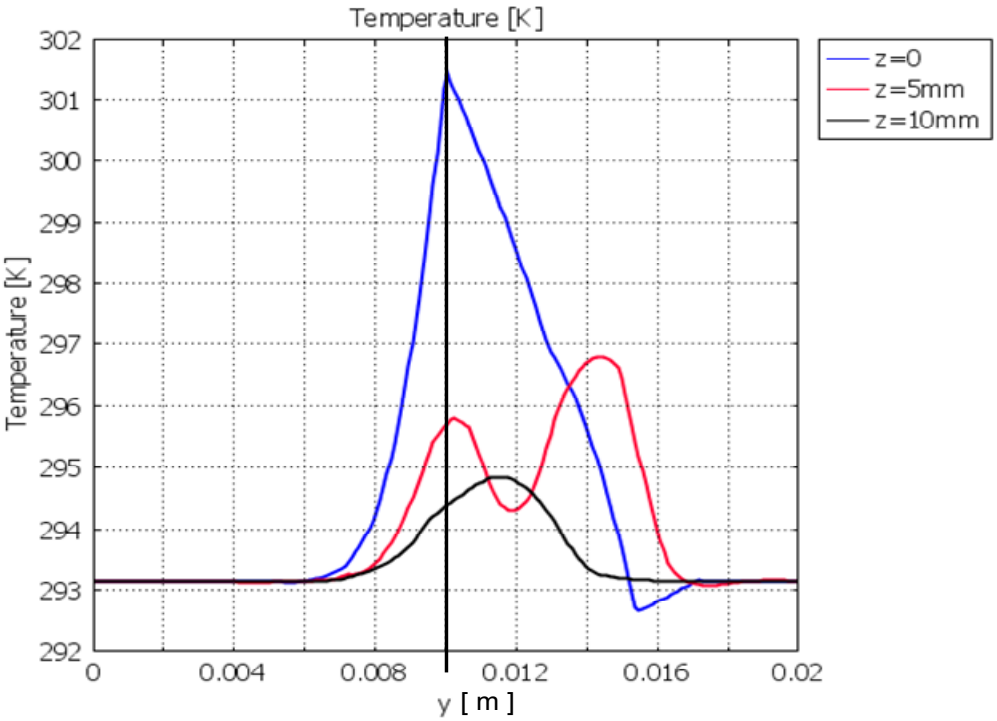

Figure 12. Results for the three-dimensional problem 1 are given. Temperature profiles as a function of y along the central vertical axis (x = 0.01m) are shown for time equals three seconds. Results are presented for various values of z. Note the asymmetry in the y-direction; this illustrates effects of vertical convection. The dip in temperature below 293K is caused by a small computational inaccuracy.

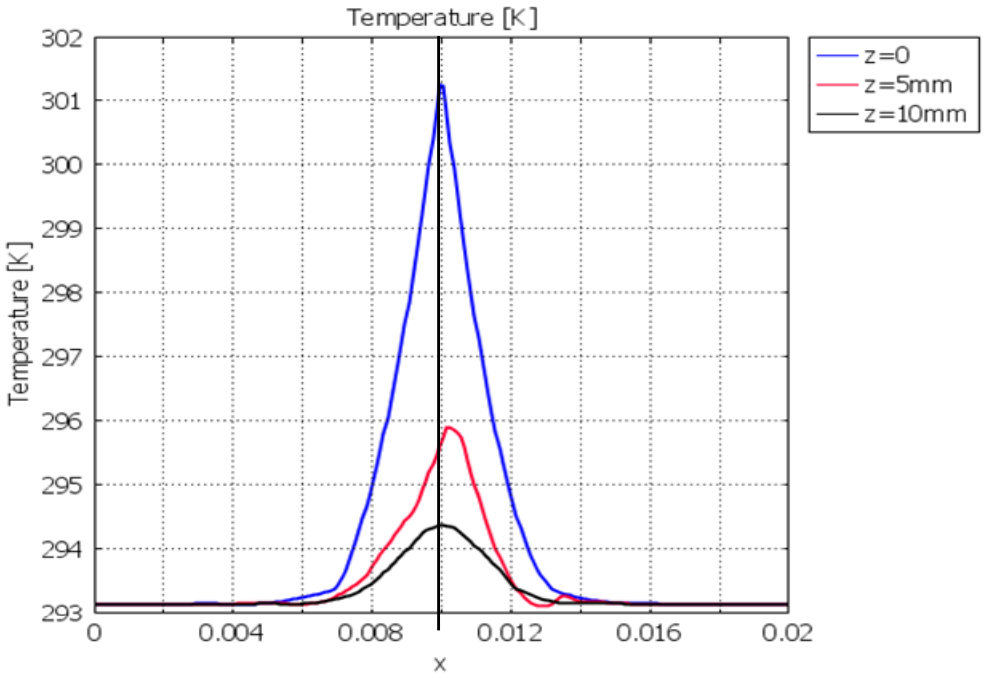

Figure 13. Results for the three-dimensional problem 1 are given. Temperature profiles as a function of x along the central horizontal axis (y = 0.01) at time equals three seconds are shown. Results are presented for various values of z. These results were plotted as a check for the evaluation of the horizontal symmetry of the solution.

4.1.1 ENERGY-CONSERVATION CHECKS OF THE SOLUTIONS OF THREE-DIMENSIONAL PROBLEM 1

In three-dimensional problem1, all surfaces are specified to be rigid and thermally insulated; therefore, energy conservation is easily accounted for within the enclosed volume of the container. Energy conservation principles, involving the first law of thermodynamics, can be used as a means of checking the results of this problem[***]. Since no external work is performed by the fixed surfaces, and there is no heat loss from the thermally insulated surfaces, according to the first law of thermodynamics,

Energy Input = Internal Energy Increase (for any time duration, t_d),

When the laser power input is constant, during a laser time duration, t_d , the energy input is given as

$$\text{Energy Input} = t_d \iiint_{Vol} \dot{Q}_s(\mathrm{x},\mathrm{y},\mathrm{z})\, dV \,, \tag{11}$$

integrated over the volume of the container.

The Energy Input [J] can be determined by substituting equations (4) and (5), with the parameters given in table 1, into the integral expression (11). Evaluating the integral over the rectangular volume of the container, we get the result for a laser time duration t_d and input laser power, *P*:

$$\boldsymbol{E_i} \;=\; P\, t_d \; erf\left(\frac{L_X}{2R_W}\right) erf\left(\frac{L_Y}{2R_W}\right)\left[1 - e^{-\mu_a L_Z}\right], \tag{12}$$

where *erf( )* denotes the error function. Substituting μ_a = 150 m^{-1}, P equals 1W, R_W equals1.5 (10^{-3}) m with the container dimensions: L_X equals 0.02m, L_Y equals 0.02m, and L_Z equals 0.04 m, we get the following result the energy input during time duration, t_d :

$$\boldsymbol{E}_\mathrm{i} = 0.9975\ t_d \tag{12a}$$

The internal energy increase [J] of the liquid during the laser time duration t_d [s] can be calculated as

$$\text{Internal Energy Increase} = \rho C \iiint_{Vol} \left[T(x,y,z) - T_0\right] dV \,, \tag{13}$$

[***] For the small convective velocities involved, viscous dissipation of energy can be neglected.

where T(x,y,z) is the calculated temperature at time t_d, and T_0 is the specified initial temperature (T_0 = 293.15K). The integration is over the volume of the container.

The internal energy increase is determined by substituting ρ = 1000 kg/m^3, C equal to 4200 J/(kg•K) and the initial condition, T_0 equal to 293.15K, into the integral expression (13) . Here the integral is evaluated using the post-processing capability of COMSOL software, where a numerical integration is performed using the evaluated results for T(x,y,z).

Calculated results for input energy, internal energy increase, and the percent difference between the energy input, E_i, and the internal energy increase in are shown in terms of the specified time durations in table 2. These results appear to show reasonable agreements between the calculated energy input and the calculated internal energy increase, especially for laser time durations greater than one second.

Table 2: Results of the energy conservation check. Laser time duration, input energy, internal energy increase, and percent difference between the input energy and the internal energy increase of the water in the closed container.

t_d (sec)	Input Energy (Joules)	Internal Energy Increase (Joules)	Percent Difference
1	0.998	0.896	10.2
2	1.996	1.854	7.1
3	2.794	2.919	4.6
4	3.992	3.897	3.4
5	4.990	4.851	2.9
6	5.988	5.771	3.6
7	6.986	6.690	4.2
8	7.984	7.610	4.7

4.2 THREE-DIMENSIONAL PROBLEM 2: SIMULATION APPLIED TO THERMAL BOUNDARY CONDITIONS WHERE HEAT TRANSFER OCCURS AT THE FRONT SURFACE (AT Z = 0) AND ALL OTHER SURFACES ARE THERMALLY INSULATED

The problem considered in this chapter is identical to the three-dimensional problem 1, treated in section 4.1, with the exception that here heat transfer between the container and its surroundings occurs at the front surface where z = 0. Thermally-insulated thermal boundary conditions are specified on the other surfaces. Also, similar to problem 1, non-slip fluid-dynamic boundary conditions are specified on all surfaces. The x-y faces are perpendicular to the laser beam. The laser beam enters perpendicularly at the center of the front face at z = 0, and the laser penetrates with exponential decay in the z-direction. As illustrated in figure 8, the faces perpendicular to the laser beam have specified dimensions $0 \le x \le 0.02$ m, and $0 \le y \le 0.02$ m and the penetration distance extends from z = 0 to z = 0.04 m. The parameters specified in table 1 apply.

The heat transfer at the z=0 surface is described by Newton's Law of Cooling [Incropera, et al, 2007; Wolfram Research, 2006]. The initial temperature in the container is 293.15K, and the initial velocity is zero everywhere. Convective heat exchange occurs between the surface at z=0 and the surroundings, which are at a fixed temperature of 293.15K. The thermal boundary condition at the z=0 surface is specified with a heat-transfer rate of $\dot{Q}_{surf}$ [W/m^2]:

$$\dot{Q}_{surf} = -he\,(T\,|_{z=0} - 293.15)\,, \qquad (14)$$

where $T|_{z=0}$ is the temperature of the fluid at z = 0^+, and the parameter he is specified as he = 15 [W/(m^2•K] [**] The boundary value, $T|_{z=0}$, interactively computed at z = 0, is dependent upon the coordinates x and y and time t. The sign convention is that heat flow into the fluid at the z = 0 boundary is positive; this explains the minus sign in equation (14).

The simulated results are obtained using Comsol finite-element software with 27,793 degrees of freedom; 969 mesh points; and 4310 tetrahedral elements.

The temperature profile at the front face (where z=0), at time equals four seconds, is shown in figure 14. A horizontal centerline is drawn to illustrative vertical asymmetry (about the central horizontal axis at y = 0.01m) due to vertical convection. A vertical centerline is drawn to evaluate the expected symmetry in the horizontal direction.

The temperature profile through the central vertical y-z plane (where x = 0.01m) at time equals four seconds is shown in figure 15. Here, the horizontal line is drawn to show vertical asymmetry in temperature due to thermal convection.

Figure 16 shows the calculated temperature profiles along the vertical central axis (at x=0.01m) at the front surface (z = 0) at various times. Figure 17 shows the calculated temperature profiles, at various values of z, as a function of y along the central vertical axis (where x=0.01) at time equals four seconds. The vertical center, at y=0.01m, is drawn on figures 16 and 17 to illustrate the vertical asymmetry of the calculated temperature profiles.

Temperature profiles as a function of x along the central horizontal axis (where y = 0.01m) at time equals four seconds are shown for various values of z in figure 18. These results are plotted as a check to evaluate the horizontal symmetry of the solution. The results demonstrate the near horizontal symmetry (about the central position at x = 0.01 m) of the calculated temperature profiles. Slight deviations from perfect horizontal symmetry can be attributed to small inaccuracies in the computational method.

[**] The value specified by the parameter he is arbitrary. The value of he=15 corresponds to the heat-transfer coefficient from skin to air. The value of he for the air/container interface is dependent upon the thermal-insulation properties of the wall of the container and its surroundings. Since this value is unknown, a value of he=15 is chosen here.

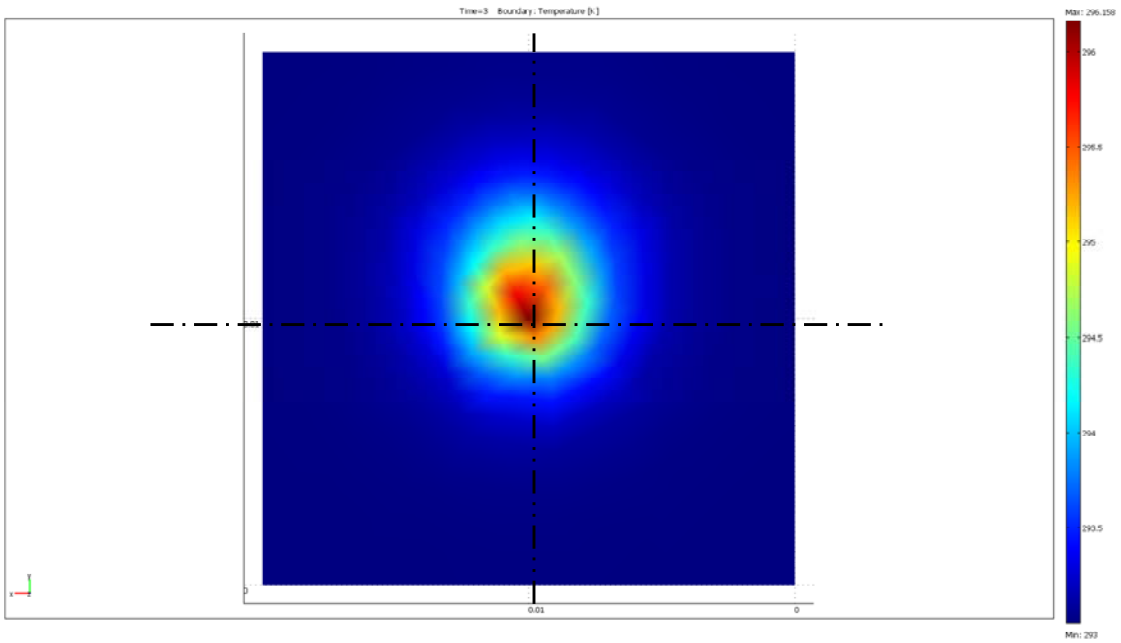

Figure 14. Results for three-dimensional problem 2 are given. The temperature profile at the front face at time equals four seconds is shown. A horizontal centerline is drawn to illustrate vertical asymmetry (about the central horizontal axis) due to thermal convection. A vertical centerline is drawn for the evaluation of the expected symmetry in the horizontal direction. Maximum temperature equals 296.2 K; minimum temperature equals 293.15K

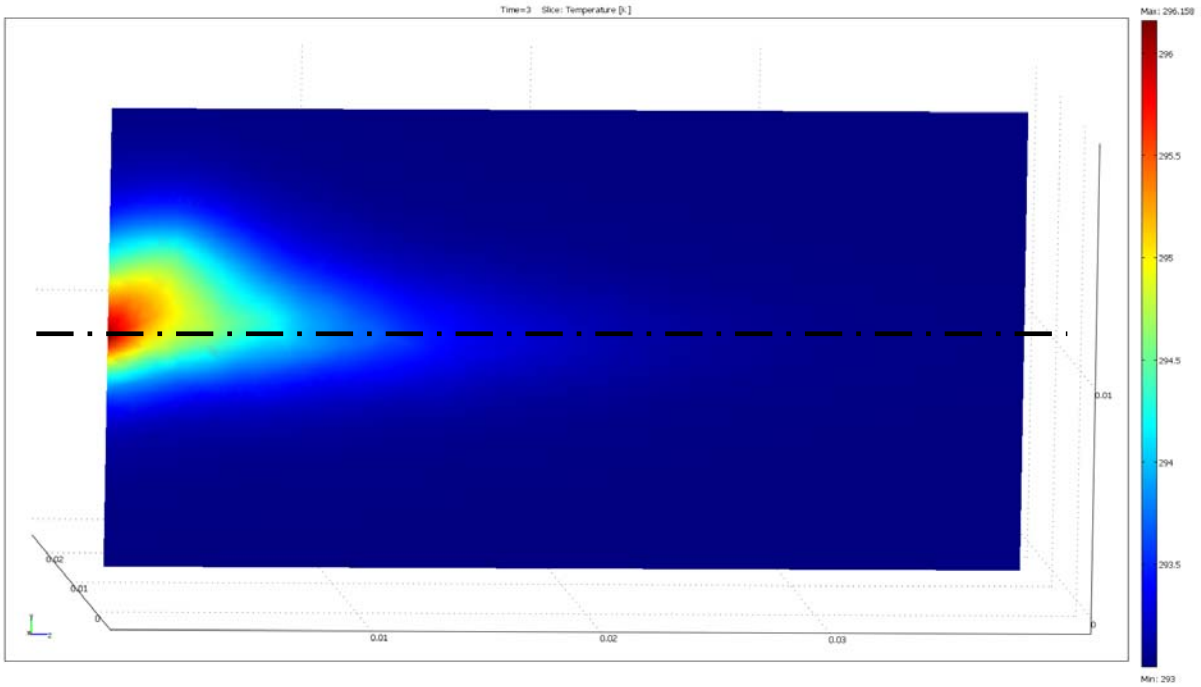

Figure 15. Results for three-dimensional problem 2 are given. The temperature profile through the central vertical plane (at x = 0.01m) at time equals four seconds is presented. The horizontal line is drawn to show vertical asymmetry due to convection. Maximum temperature equals 296.2K; Minimum temperature equals 293.15K.

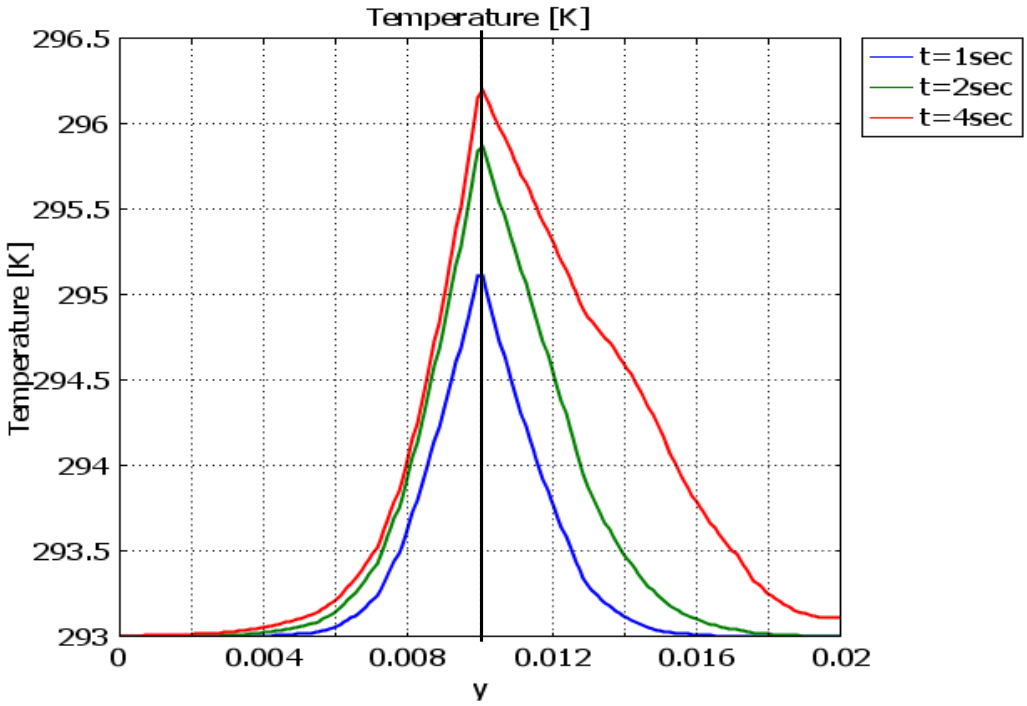

Figure 16. Results for three-dimensional problem 2 are given. The temperature profiles along the vertical central axis (at x = 0.01m) at the front face (where z = 0) at various times are presented

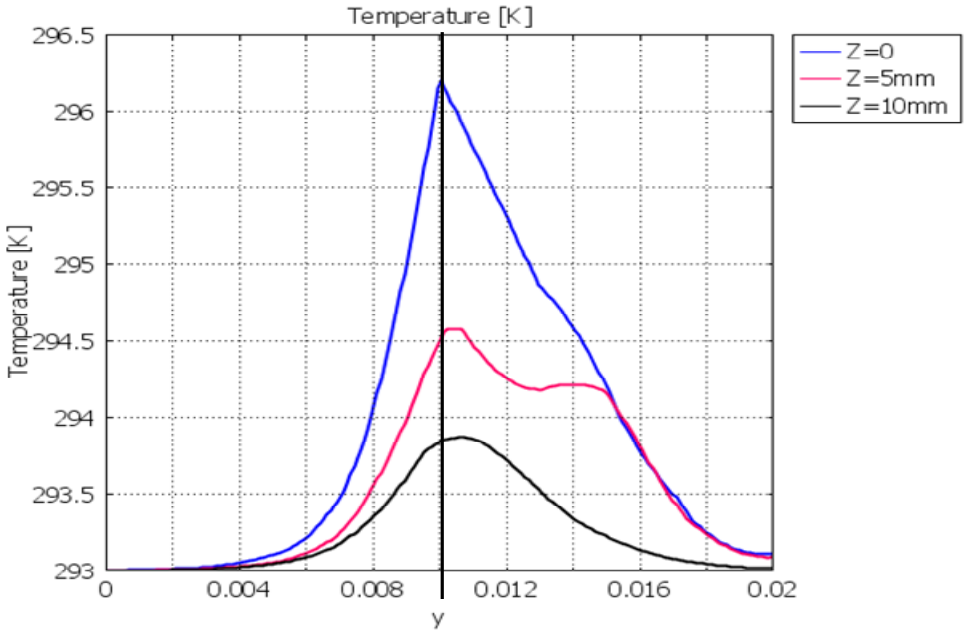

Figure 17. Results for three-dimensional problem 2 are given. The temperature profiles, as a function of y, along the central vertical axis (where x = 0.01) at time equals four seconds are presented. Results are shown for various values of z. Note the asymmetry in the y-direction; this illustrates effects of vertical convection.

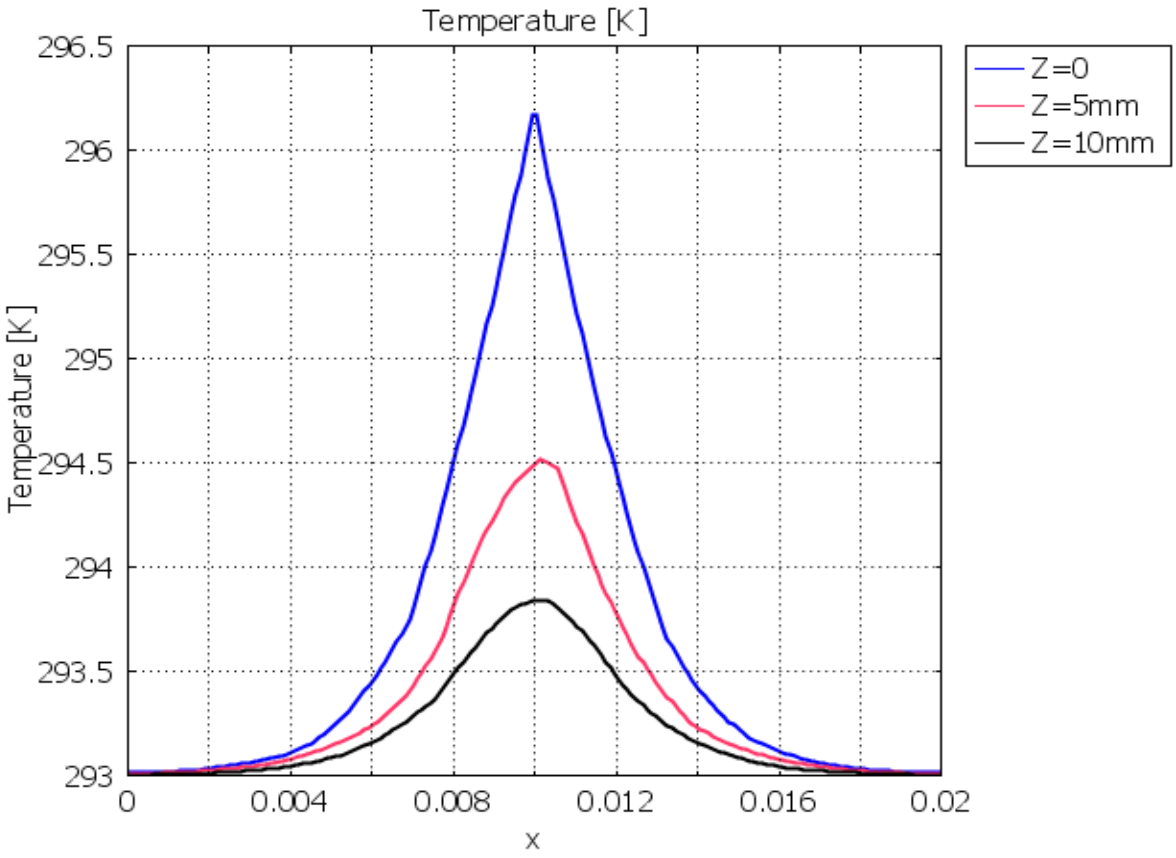

Figure 18. Results for three-dimensional problem 2 are given. Temperature profiles as a function of x along the central horizontal axis (y = 0.01) at time equals four seconds are presented. Results are shown for various values of z. These results are plotted as a check for the evaluation of the horizontal symmetry of the solution.

5. FREE-SURFACE EFFECTS

The problems described in chapter 4 involve heat transfer in closed containers. For the problem considered in section 4.1, all boundaries are thermally insulated. For the problem considered in section 4.2, convective heat transfer occurs between the front boundary (at z = 0) and its surroundings. The fluid-dynamic boundary conditions for problems described in sections 4.1 and 4.2 involve zero velocity at the walls (the non-slip conditions for fixed surfaces).

In this chapter, the effects of free-surface boundary conditions are discussed. These surface effects include convective and evaporative heat transfer and surface-tension induced by temperature gradients on the surface (the Marangoni Effect).

5.1 EVAPORATIVE AND CONVECTIVE HEAT TRANSFER AT A FREE SURFACE:

Two mechanisms of energy exchange can take place at the air-liquid surface, at z = 0. One mechanism involves the convective heat transfer between the liquid at density ρ_L (kg/m^3) and the vapor at density ρ_v (kg/m^3). The other mechanism involves heat loss from water evaporation at z = 0 [Tilbas and Sami, 1998]. Thus, the thermal boundary condition at z = 0 (at the air-water interface) is

$$k \left.\frac{\partial T}{\partial Z}\right|_{Z=0} = \dot{Q}_{vap} + \dot{Q}_{surf} \cdot \tag{15}$$

The heat evaporation term, $\dot{Q}_{vap}$ [W/m^2], at z = 0 is

$$\dot{Q}_{vap} = h_{fg} h_m \left(\rho_{v(sat)} - \rho_{v(inf)}\right). \tag{16}$$

Here h_{fg} is the parameter representing enthalpy change due to evaporation (J/kg), h_m is the mass-transport coefficient (m/s), $\rho_{v(sat)}$ is the mass density of the water vapor at the water surface, and $\rho_{v(inf)}$ is the mass density of the water vapor at the room temperature. The convective heat transfer term at z=0, $\dot{Q}_{surf}$, is given by equation (14).

Consider a cylindrical column of water with a laser beam heat source and with heat transfer due to evaporation and convection at the top (z = 0) surface as shown in figure 19.

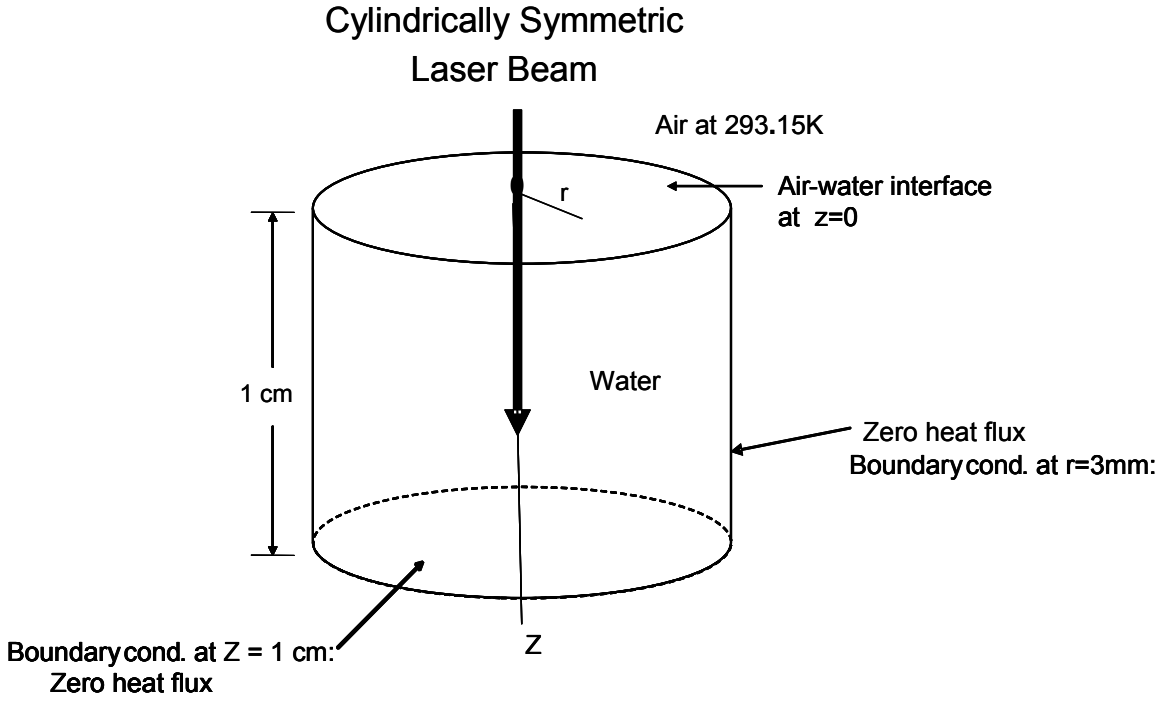

Figure 19. The geometry for the simulation involving the evaporative and convective heat transfer at the z = 0 surface is illustrated. The height of the cylinder equals 1 cm, and the radius of the cylinder equals 0.5 cm. The laser beam enters perpendicularly at the top (at z = 0) surface. The problem is circularly symmetric.

The heat conduction equation is

$$\rho c \frac{\partial T}{\partial t} - \nabla \bullet \left(k \nabla T \right) = \dot{Q}_S \,. \tag{17}$$

For simplicity, heat convection within the fluid is not considered in this chapter.

The heat source term, $\dot{Q}_S$, is described by equations (4) and (5) (with appropriate alterations corresponding to the cylindrical geometry for the problem solved in this chapter). The problem is solved in cylindrical coordinates with axial symmetry.
The problem is solved using COMSOL software. As evaporation takes place, the water layer is depleted at the evaporative surface at z=0. To account for the depleted water layer, the problem is solved with moving coordinates (moving boundaries). That is, at z=0, the mass depletion per unit surface area per unit time (kg/(m^{2}s)) is calculated as

$$\dot{M} = \mathrm{h_m} \left(\rho_{\mathrm{v(sat)}} - \rho_{\mathrm{v(inf)}} \right). \tag{18}$$

The surface velocity of the moving boundary at z = 0 is

$$v_Z\big|_{z=0} = \frac{\dot{M}}{\rho_L}, \tag{19}$$

where ρ_L is the density of the liquid water at the evaporating surface.

The parameters describing this problem are shown in Table 3a, and the relations used are shown in Table 3b. The simulated results are obtained using Comsol finite-element software with 3,271 degrees of freedom; 277 mesh points; and 406 triangular elements.

Results showing the temperature profiles at time equals eight seconds are shown in figure 20. Alterations in the shape of the top surface were small and were not apparent in figure 20 for the incident laser power (1W) considered. Alterations in the shape of the top surface would be observed if higher laser power were used in the simulation.

Table 3a. Parameters describing the free-surface problem

Parameters	Value	Description
Tinf	293.15	Room Temp (K)
he	15	Heat convection coeff (W/m^2K)
hfg	2.35e6	phase-change enthalpy (J/kgK)
Rh	0.50	Relative humidity
rho_v_sat_inf	0.0173	mass density of saturated water vapor at room temperature
P_beam	1	Laser power (W)
mu	150	absorption coeff (m^-1)
R_W (R_waist)	0.0015	beam waist size (m)
Rho_L	1,000	density of liquid water (kg/m^3)
T_room	293.15	room temp (K)

Table 3b. Relations between the expressions describing the evaporation problem

Expressions

Term	Expression	Description
hm	he*(1e-6*Tcc+0.0009)	Convection mass transfer coeff (m/s)
Qsource	2.*P_beam/(pi*r_waist^2)*exp(-2.*r^2/(r_waist^2))*exp(-mu*z)	Laser source power density (W/m^3)
Tcc	T-273	Conversion from cent. To Kelvin Temp
pho_v_sat_surf	1e-3*(4e-6*Tcc^4-6e-5*Tcc^3+0.0196e-3*Tcc^2+0.1534*Tcc+6.1098)	Density of saturated water vapor at z=0 surface
Qvap	hfg*hm*(pho_v_sat_surf-rho_v_sat_inf)	Evap surface heat losses (W/m^2)
Qconv_surf	he*(T-Tinf)	Conv. surface losses (W/m^2)

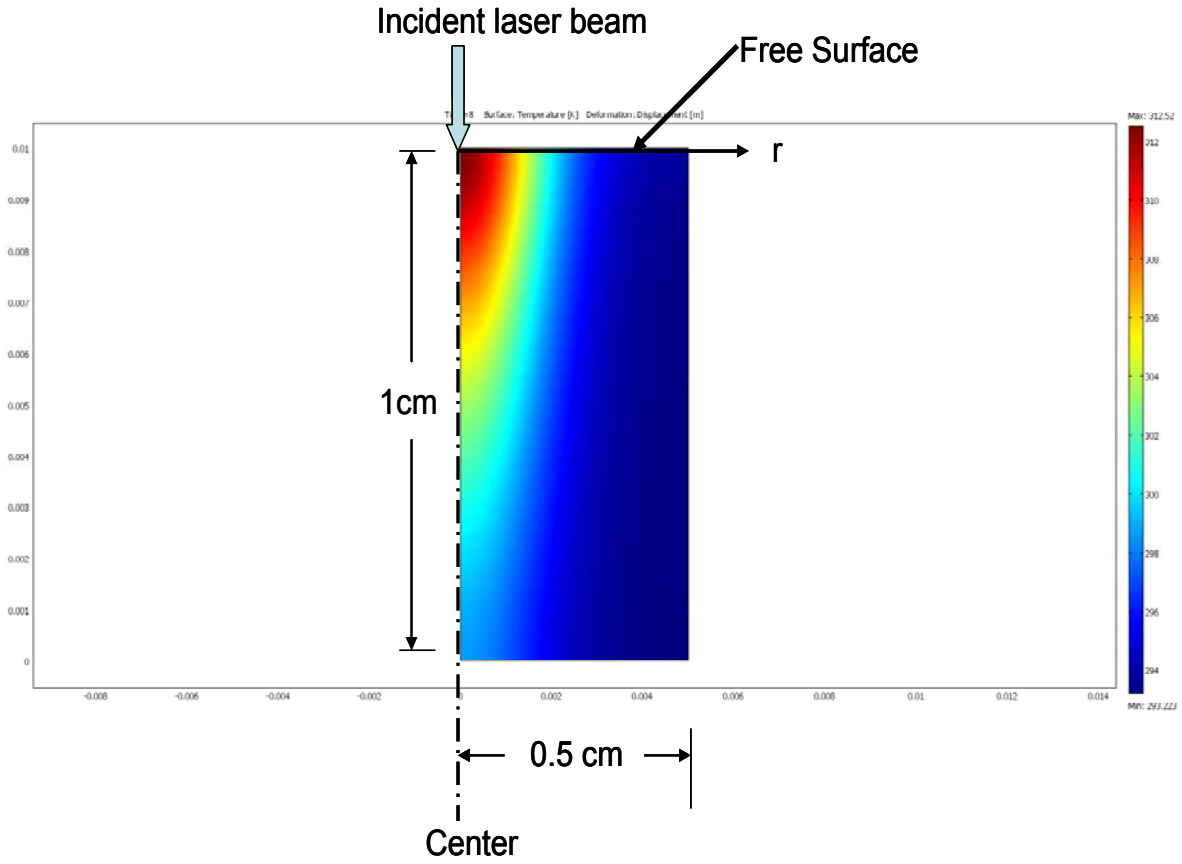

Figure 20. The simulated temperature profile in a cylindrical container of water is shown. Evaporative cooling and convective heart exchange take place at the top boundary, where z equals zero. Results for time equals eight seconds are presented. Laser input power equals 1W. Maximum temperature equals 312K; Minimum temperature equals 293.15K

5.2 SURFACE TENSION AT A FREE SURFACE: THE MARANGONI EFFECT

Surface tension at the surface of a liquid may be caused by radius-of-curvature variations along the surface and/or by temperature gradients along the surface [Pimputkar and Ostrach., 1980].

The production of surface tension by variations of the radius of curvature along a surface is described by Laplace's Law [Landau and Lifshitz, 1959]. This effect is commonly small for the temperature range considered in this report.

The production of surface tension by temperature gradients along a free surface is described as the Marangoni Effect [Levich, 1962; Levich and Krylow, 1969; Longtin et al, 1999]. The surface boundary condition at the liquid-air interface is given in terms of the surface stresses that are produced by Marangoni convection; these stresses at the liquid-air interface are given as

$$\eta \frac{\partial u_x}{\partial y} = \gamma \frac{\partial T}{\partial x} \tag{20}$$

where x is the direction tangent to the surface and y is the direction normal to (and into) the surface. The parameter γ is equal to the derivative of the surface tension with respect to temperature. A plot of the surface tension vs. temperature of water is shown in figure 21. The parameter γ is determined by taking the derivative with respect to temperature of the curve shown in Figure 21.

The surface tension would drive fluid flow at and near the free surface [Yih, C.S, 1968, 1969]. A simulation showing the flow induced by Marangoni convection is given in the COMSOL Multiphysics Modeling Guide [2005].

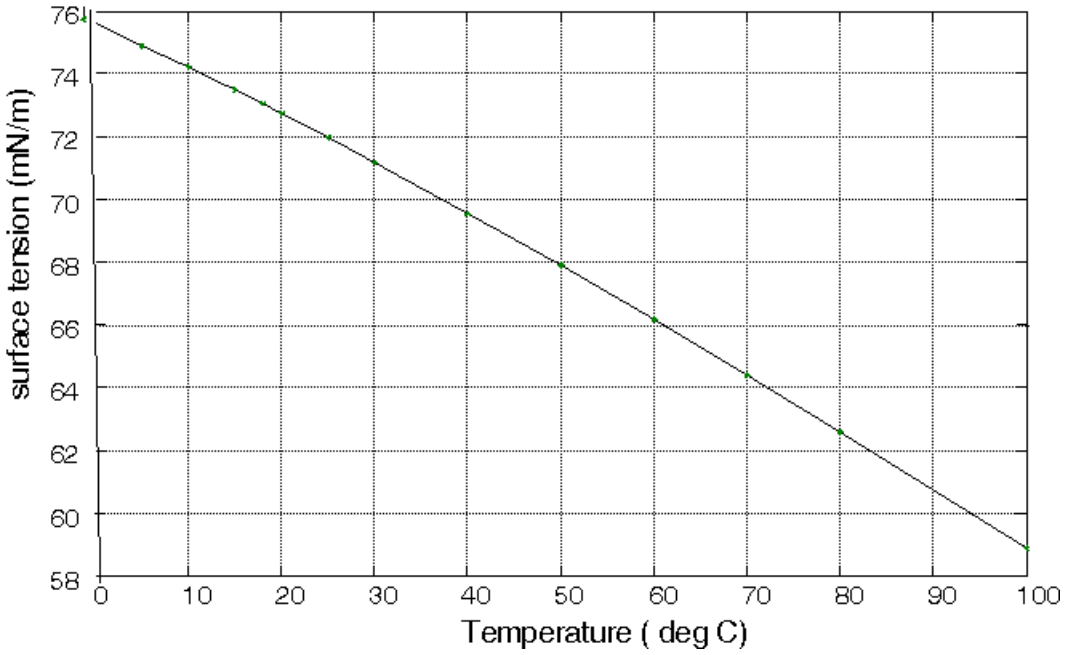

Figure 21. Surface tension vs. temperature of water. The value of the parameter γ can be found by taking the derivative of this curve.

6. SUMMARY

Mathematical models and their simulated results are presented to describe heat transfer from a penetrating laser beam in a rectangular container of water. Beer's law is used as an approximation of the absorption loss of the laser beam, and scattering effects are neglected. Both convective and conductive heat transfer are considered. COMSOL software is used to find finite-element simulation results for convective flow velocity and temperature changes within the container. Both simulated results and dimensional analysis indicate that convective flow is important.

The following suggestions are made concerning the manner in which this work can be extended in future investigations:

1. The simulated temperature changes could be coupled with calculated optical effects in which changes of refractive index with temperature can be taken into account. The importance of thermal convection on the optical measurements has been suggested in experiments by Vincelette et al [2007].

2. The simulated temperature changes should be verified experimentally. For this purpose, the temperature mapping methods of Maswadi et al [2004] could be used.

3. The work can be extended to incorporate surface phenomena, as described in chapter 5, with the heat conduction/convection simulations presented in chapter 4.This work can be further extended to include the simulation of temperature changes and the associated changes in the optical properties of a tear film at the surface of the cornea of the eye.

This page intentionally left blank

7. REFERENCES

Acheson, D.J., Elementary Fluid Dynamics, Clarendon Press (Oxford University press), 1990.

Batchelor, G. K. An Introduction to Fluid Dynamics, Cambridge University Press, 1967.

Gebhart, B., Pera, L., Schorr, A.W., Steady laminar natural convection plumes above a horizontal line heat source, International Journal of Heat and Mass Transfer, vol. 13, pp. 161-171, 1970.

CONSOL Lib. Comsol Fluid Parameter Library, Comsol, Inc. (This library is internal to the COMSOL software package.), 2007.

COMSOL Multiphysics Modeling Guide, v.3.2, 2005.

Drazin, P.G. and Reid, W.H., Hydrodynamic Stability, Cambridge university press, 1981.

Incropera, F.P., Dewitt, DP, Bergman, T.L., and Levine, A.S., Fundamentals of Heat and Mass Transfer, 6th Ed., Wiley Press, 2007.

Landau, L.D. and Lifshitz, E.M., (Translated by Sykes, J.B. and Reid, W.H.) Fluid Mechanics, Pergamon Press, 1959.

Levich, V.G., Physicochemical Hydrodynamics, Prentice Hall, 1962.

Levich, V.G., Krylow V.S., Surface-Tension-Driven Phenomena, Ann Rev of Fluid Mechanics, vol. 1, pp. 293-316, January 1969.

Longtin, J.P., Hijikata, K., Ogawa, K., Laser-induced surface-tension-driven flows in liquids, International Journal of Heat and Mass Transfer, vol. 42, pp. 85-93, 1999.

Maswadi, S.M., Dodd, S.J., Glickman, R.D., Temperature mapping of laser-induced hyperthermia in an ocular phantom using magnetic resonance, Journal of Biomedical Optics, vol. 9, no. 4, pp. 711-718, July/August 2004.

Pimputkar, S.M., Ostrach, S., Transient thermocapillary flow in thin liquid layers, Physics of Fluids, vol. 23, no. 7, pp. 1281-1285, July 1980.

Reddy, J.N. and Gartling, D.K., The Finite Element Method in Heat Transfer and Fluid Dynamics, CRC Press, 2nd edition, 2001.

Roider, J., Birngruber, R., Soultion of the Heat Conduction Equation, in Optical-Thermal Response of Laser-Irradiated Tissue, (A.J. Welch and M.J.C. van Gemert), pp. 411-443, Plenum Press, 1995.

Somogy, D., Surface Tension Waves, Physics Department, The College of Wooster, pp. 1-2, May 2002.

Tilbas, B.S., Sami, M., Three-dimensional laser heating including evaporation – a kinetic theory approach, International Journal of Heat Mass Transfer, vol. 41, no. 13, pp. 1969-1981, 1998.

Torres, J.H., Motamedi, M., Pearce, J.A., and Welch, A.J., Experimental Evaluation of Mathematical Models for Predicting the Thermal Response of Tissue to Laser Irradiation, Applied Optics, vol. 32, no. 4, pp. 597-606, Feb. 1993.

Tritton, D.J., Physical Fluid Dynamics, 2nd ed., Oxford Univ. Press., 1998.

Velarde, M.G., and Normand, C., Convection, Scientific American, vol. 243 (1), pp. 92-108, 1980.

Vest, C.M., Analysis of laser-induced convection in unconfined fluids and in vertical cylinders, The Physics of Fluids, vol. 17, no. 11, November 1974.

Vincelette, R.L., Thomas, R.J., Rockwell, B.A., and Welch A.J., Thermal Lensing in the Ocular Media, in Optical Interactions in Biomedical Optics and Imaging, vol.8, no. 2, Optical Interactions With Tissue and Cells XVIII, (Jacques, S.L. and Roach, W.P. Editors) Spie Volume 6435, pp. 64350C-1 to 64350C-7, , San Jose, CA, 22-24 January 2007.

Vrentas, J.S., Narayanan, R., Agrawal, S.S., Free surface convection in a bounded cylindrical geometry, International Journal of Heat and Mass Transfer, vol. 24, no. 9, pp. 1513-1529, 1981.

Wolfram Research, Newton's Law of Cooling, scienceworld.wolfram.com, 2006.

Yih, C.S., Fluid Motion Induced by Surface-Tension Variation, The Physics of Fluids, vol. 11, no. 3, pp. 477-480, March 1968.

Yih, C.S., Three-dimensional Motion of a Liquid Film Induced by Surface-Tension Variation or Gravity, The Physics of Fluids, vol. 12, no. 16, October 1969.

Zimmerman, W.B., Multiphysics Modeling With Finite Element Methods, World Scientific Publishing, 2006.

ACKNOWLEDGEMENTS

The P.I. wishes to acknowledge the support from the Air Force Research Laboratory, grant number FA8650-06-1-6747. The PI also wishes to thank Dr. Taufiquar R. Kahn at Clemson University for his suggestions.